

Signaling networks and cell motility: a computational approach using a phase field description

Wieland Marth · Axel Voigt

Received: 10 July 2012 / Revised: 27 May 2013
© Springer-Verlag Berlin Heidelberg 2013

Abstract The processes of protrusion and retraction during cell movement are driven by the turnover and reorganization of the actin cytoskeleton. Within a reaction–diffusion model which combines processes along the cell membrane with processes within the cytoplasm a Turing type instability is used to form the necessary polarity to distinguish between cell front and rear and to initiate the formation of different organizational arrays within the cytoplasm leading to protrusion and retraction. A simplified biochemical network model for the activation of GTPase which accounts for the different dimensionality of the cell membrane and the cytoplasm is used for this purpose and combined with a classical Helfrich type model to account for bending and stiffness effects of the cell membrane. In addition streaming within the cytoplasm and the extracellular matrix is taken into account. Combining these phenomena allows to simulate the dynamics of cells and to reproduce the primary phenomenology of cell motility. The coupled model is formulated within a phase field approach and solved using adaptive finite elements.

Keywords Cell motility · Reaction–diffusion · Phase-field approximation

Mathematics Subject Classification 92C17 · 35K57 · 74K15 · 76D45

1 Introduction

Cellular shapes change dynamically in striking ways as a result of mechanical interactions and complex reactions both within the cytoplasm and on the cellular membrane.

W. Marth · A. Voigt (✉)
Department of Mathematics, TU Dresden, 01062 Dresden, Germany
e-mail: axel.voigt@tu-dresden.de

W. Marth
e-mail: wieland.marth@tu-dresden.de

Many theoretical studies consider only the mechanical part. They are based on the Helfrich Hamiltonian (Helfrich 1973) and consider only the elastic properties of the membrane accounting for bending and surface tension. Within such an approach the membrane is considered as an elastic sheet and its evolution is driven by energy minimization. Various mathematical approaches have been used to solve this problem, see e.g. Du et al. (2005a), Du et al. (2006), Du and Zhang (2008), Elliott and Stinner (2010), Lowengrub et al. (2009) and the references therein. Combining the Helfrich Hamiltonian with streaming effects in the cytoplasm and the extracellular matrix, as e.g. considered in Bonito et al. (2011), Du et al. (2007), Du et al. (2009), Lowengrub et al. (2007), Ryham et al. (2012), and Sohn et al. (2010) leads to more realistic dynamical models, but still focusing only on the mechanical part of the problem. In McMahon and Gallop (2005) different mechanisms leading to cell deformation are described. One of the key ingredients is the cytoskeletal assembly and disassembly. Cell shape is thereby formed by three primary polymer systems that make up the cytoskeleton: the actin filaments, intermediate filaments and microtubules. The actin polymerization thereby has a force generating role during cell motility and the branching, bundling and treadmilling of actin filaments plays a crucial role in the generation and remodeling of high membrane curvature regions. Our goal is to combine these processes with the Helfrich Hamiltonian and streaming effects and to derive a general computational model for cell motility.

Previous attempts in this direction have e.g. been considered by Elliott et al. (2012), Maree et al. (2006), Shao et al. (2012), Shao et al. (2010), Vanderlei et al. (2011), and Ziebert et al. (2012), but non of these models accounts for the different dimensionality of the cell membrane and the cytoplasm, streaming and the Helfrich Hamiltonian.

The paper is organized as follows: In Sect. 2 we describe the crawling of cells and introduce a minimal biochemical network model for the activation of GTPase to initiate the crawling motion. We introduce the Helfrich Hamiltonian and hydrodynamic interactions and combine both to form a continuum cell motility model, which will be formulated within a phase field approach. We also briefly describe the numerical approach to solve the coupled system and validate it. Simulation results are discussed in Sect. 3, which include the formation of lamellipodia and filopodia-like structures, the response of the cell according to a chemoattractor in the extracellular matrix and various parameter studies on the influence of bending rigidity and surface tension. Conclusions are drawn in Sect. 4, which also includes a discussion of generalizations of the model and extensions towards specific cell types.

2 Cell polarity as a result of a Turing type instability

All crawling cells move by first protruding a cell front and subsequently retracting the cell rear. The processes of protrusion and retraction are both driven by the turnover and reorganization of the actin cytoskeleton. Two abilities of actin filaments are exploited by the cell in order to move: the ability to push by polymerization and the ability to contract by interacting with myosin. Actin polymerization drives the extension of sheet-like and rod-like protrusions at the cell front, termed respectively lamellipodia and filopodia. Behind the protruding front actin interacts with myosin

to form contractile arrays that drive the translocation of the trailing cell body. To model these phenomena an understanding of the processes leading to actin polymerization and actin-myosin interaction is required, which can be described through protein interactions.

Proteins associated with actin are generally classified as actin binding-, actin associated- or actin modulating-proteins. They play key roles in determining the organization of actin filaments into the different organizational forms found in the actin cytoskeleton. Members of the Rho family of small GTPases have been shown to operate in distinct pathways signaling the formation of different organizational arrays of the actin filaments in the actin cytoskeleton. Rac and Cdc42 signal the formation of lamellipodia and filopodia, respectively, and Rho signals the formation of actin stress fibre bundles for the cell retraction. We thus need a detailed signaling network of small GTPases with the ability to distinguish between cell front and rear, which can be achieved through polarization. Various models have been proposed, see [Jilkiné and Edelstein-Keshet \(2011\)](#) for a review and comparison of mathematical models for single eukaryotic cells. One of the most detailed models is based on a Turing-type instability [Goryachev and Pokhilko \(2008\)](#). Such models are attractive to consider, as the Turing instability can lead to spontaneous polarization, a high degree of amplification can be achieved and the polar pattern remains after the signal is removed. However, such a diffusion driven instability typically requires large differences in the diffusion coefficient of the involved species. This might not be realistic in our case as diffusion coefficients for proteins are similar to each other. However, diffusion along the cell membrane and within the cytoplasm can be different. Also association and disassociation between the cell membrane and the cytoplasm might differ for various proteins. Taking these processes into account might form more realistic Turing mechanism [Levine and Rappel \(2005\)](#). Models which distinguish between cytoplasm and cell membrane have already been proposed for the emergence of cell polarity. In [Altschuler et al. \(2008\)](#) a model of positive feedback is considered in which a single species of diffusible, membrane-bound signaling molecules can self-recruit from a cytoplasmic pool. In this model the polarization frequency has an inverse dependence on the number of signaling molecules. The frequency of polarization decreases as the number of molecules becomes large, which suggests that positive feedback can work alone or with additional mechanisms to create robust cell polarity. The results of [Wedlich-Soldner et al. \(2004\)](#) on the regulation of GTPase Cdc42 suggest that cell polarity is established through coupling of transport and signaling pathways and maintained actively by balance of flux between the cytoplasm and the membrane. A similar cytoskeleton-dependent mechanism that could account for the intrinsic ability of cells to polarize in response to Cdc42 activation was proposed in [Wedlich-Soldner et al. \(2003\)](#) and [Maree et al. \(2006\)](#). The mechanism involves a positive feedback loop between Cdc42-dependent actin polymerization and delivery of Cdc42 to the plasma membrane. A detailed model for signaling networks of the GTPase cycle accounting for the coupling of membrane bound and cytoplasmic processes has been shown to lead to a Turing instability in [Rätz and Röger \(2012\)](#). Here the different dimensionality of the membrane and the cytoplasm is taken into account in the reaction–diffusion processes. Mathematically the model considers diffusion in the cytoplasm with a reaction–diffusion system along the membrane serving as a boundary condition. The

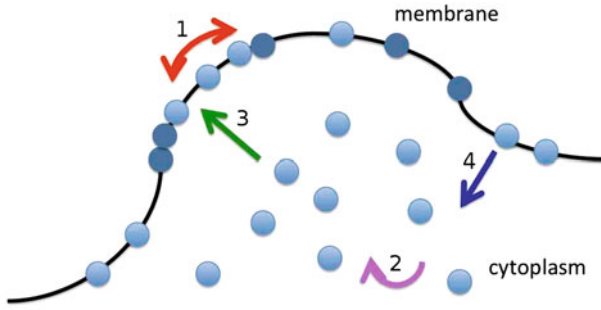


Fig. 1 Schematics of GTPase cycle. *Arrows indicate various molecular transport mechanisms: red (1) diffusion along the membrane, purple (2) diffusion within the cytoplasm, green (3) association with the membrane, blue (4) disassociation from the membrane*

model distinguishes between membrane-bound active and inactive state of the GTPase, for which the concentrations are denoted by c_1 and c_2 , respectively, and complexes of cytoplasmic GTPase, denoted by C , see Fig. 1 for a schematic description.

The model accounts for activation of GTPase by exchange of GDP by GTP, and inactivation by hydrolysis and dephosphorylation of GTP to GDP, which are catalyzed by GEF and GAP protein, respectively. The resulting model reads in dimensionless form

$$\partial_t C + \nabla \cdot (C\mathbf{u}) = D_C \Delta C \tag{1}$$

$$\begin{aligned} \partial_t c_1 + \mathbf{u} \cdot \nabla c_1 - \mathbf{u} \cdot \nabla_\Gamma c_1 + c_1(\mathbf{u} \cdot \mathbf{n})(\nabla_\Gamma \cdot \mathbf{n}) \\ = -\nabla_\Gamma \cdot (c_1(\mathbf{I} - \mathbf{n} \otimes \mathbf{n})\mathbf{u}) + d_{c_1} \Delta_\Gamma c_1 + \gamma h(c_1, c_2) \end{aligned} \tag{2}$$

$$\begin{aligned} \partial_t c_2 + \mathbf{u} \cdot \nabla c_2 - \mathbf{u} \cdot \nabla_\Gamma c_2 + c_2(\mathbf{u} \cdot \mathbf{n})(\nabla_\Gamma \cdot \mathbf{n}) \\ = -\nabla_\Gamma \cdot (c_2(\mathbf{I} - \mathbf{n} \otimes \mathbf{n})\mathbf{u}) + d_{c_2} \Delta_\Gamma c_2 - \gamma h(c_1, c_2) + \gamma q(c_1, c_2, C) \end{aligned} \tag{3}$$

and boundary condition

$$-D_C \nabla C \cdot \mathbf{n} = \gamma q(c_1, c_2, C) \tag{4}$$

coupling the equations along the membrane and within the cytoplasm. The first equation is valid in $\Omega_{cp}(t)$ the cytoplasm, assumed to be a bounded, connected open domain; where as the last two equations are defined on $\Gamma(t)$ the cell membrane, which is the boundary of $\Omega_{cp}(t)$, assumed to be a smooth and closed surface; and $I = [0, T]$ a time interval. All quantities are assumed to be defined off the membrane. We assume a constant extension in normal direction \mathbf{n} , which is defined to point outwards. \mathbf{I} denotes the identity matrix and \mathbf{u} the velocity of the moving cell. The terms containing \mathbf{u} in the equations account for convection and stretching effects, see e.g. [Teigen et al. \(2011\)](#) for related surfactant models on a deformable surface. The reaction kinetics in the equations are denoted by

$$h(c_1, c_2) = a_1 c_2 + a_2 \frac{c_1}{b_1 + c_1} c_2 - a_3 \frac{c_1}{b_2 + c_1} \tag{5}$$

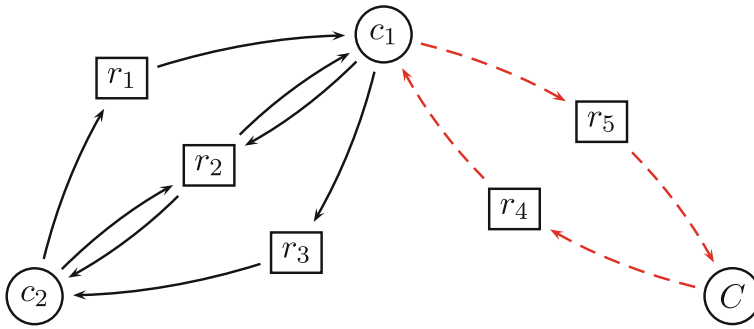


Fig. 2 Reaction network. The bipartite graph has two types of nodes, molecular species c_1 , c_2 and C , and the reactions between them, denoted by r_i , $i = 1, \dots, 5$, the index corresponds to the index of the kinetic coefficients. *Directed edges* of the graph represent the flow of the reaction fluxes. *Black (solid) edges* indicated processes on the membrane and *red (dashed) edges* processes within the cytoplasm, including association and disassociation

and the association and disassociation is modeled by

$$q(c_1, c_2, C) = a_4 C(1 - c_1 - c_2)_+ - a_5 c_2, \tag{6}$$

which follows from a Langmuir law. It models the membrane association as an reaction between the cytoplasmic GTPase complex and a free site on the membrane. $(\cdot)_+$ thereby denotes the positive part of (\cdot) . The system is given in dimensionless form with diffusion coefficients D_C , d_{c_1} and d_{c_2} in the cytoplasm and along the membrane, respectively. a_i are kinetic coefficients, b_i kinetic parameters, γ a dimensionless scaling factor. Δ_Γ is the surface Laplacian and $\nabla_\Gamma \cdot$ the surface divergence. Figure 2 shows the corresponding reaction network as a bipartite graph, distinguishing processes along the membrane and within the cytoplasm.

In Rätz and Röger (2012) the velocity terms in the equations are neglected and the system is further reduced by assuming C to be spatially constant as a result of a larger diffusivity in the cytoplasm as along the membrane. A linear stability analysis for the reduced system was shown to lead to a Turing instability for appropriate parameters, see Rätz and Röger (2012). More recently a Turing instability could also be found for the biologically more interesting regime in which $d_{c_1} = d_{c_2}$, see Rätz and Röger (2013). Now only different diffusivities within the cytoplasm and along the cell membrane as well as different association/disassociation coefficients are required to form Turing patterns. We will consider these parameters also for the evolving situation.

2.1 Hydrodynamical model for cell dynamics

We consider the cellular membrane to be an elastic material. The dynamics are modeled as a combined process of energy minimization and an active driving force. The corresponding spontaneous-curvature model (Helfrich 1973) is based on the assumption that the surface energy associated with bending of the membrane can be expanded in the dimensionless mean curvature H . The energy \mathcal{E} consists of the normal bending energy as well as a surface tension term and reads in nondimensional form

$$\mathcal{E} = \mathcal{E}_B + \mathcal{E}_S = \frac{1}{2} \frac{1}{\text{Be}} \frac{4\sqrt{2}}{3} \int_{\Gamma} (H - H_0)^2 d\Gamma + \frac{1}{\text{Ca}} \frac{2\sqrt{2}}{3} \int_{\Gamma} d\Gamma, \tag{7}$$

with H_0 the spontaneous curvature, which reflects a possible asymmetry of the membrane, justified by a different chemical environment on both sides of the membrane. It can be a function of a protein concentration, see e.g. [Veksler and Gov \(2007\)](#). Here, for convenience H_0 is assumed to be spatially homogeneous. Be denotes the dimensionless quantity associated with normal bending stiffness, the bending capillary number, and Ca is the capillary number measuring the effect of surface tension. Additional contributions, e.g. due to Gaussian curvature are neglected. For a review of models based on the spontaneous-curvature model we refer to [Haußer et al. \(2013\)](#), and [Seifert \(1997\)](#).

We now consider a two-phase flow problem with the cell membrane separating the cytoplasm $\Omega_{cp}(t)$ and the extracellular matrix $\Omega_{em}(t)$. We assume an incompressible Newtonian fluid in $\Omega_{cp}(t)$ and $\Omega_{em}(t)$ and consider equal density and viscosity for simplicity. The model thus reads in dimensionless form

$$\begin{aligned} \partial_t \mathbf{u}_i + (\mathbf{u}_i \cdot \nabla) \mathbf{u}_i &= -\nabla p_i + \frac{1}{\text{Re}} \Delta \mathbf{u}_i & (8) \\ \nabla \cdot \mathbf{u}_i &= 0 & (9) \end{aligned}$$

for velocity \mathbf{u}_i and pressure p_i , with $i = 1$ in $\Omega_{cp}(t)$ and $i = 2$ in $\Omega_{em}(t)$. Re denotes the characteristic Reynolds number. Across the interface $\Gamma(t)$, the following jump conditions hold:

$$\begin{aligned} [\mathbf{u}] &= 0 & (10) \\ \left[-p\mathbf{I} + \frac{1}{\text{Re}} (\nabla \mathbf{u} + \nabla \mathbf{u}^T) \right] \cdot \mathbf{n} &= \frac{1}{\text{Re}} \frac{\delta \mathcal{E}_B}{\delta \Gamma} + \frac{1}{\text{Re}} \frac{\delta \mathcal{E}_S}{\delta \Gamma} + \frac{1}{\text{Re}Fa} c_1 \mathbf{n}, & (11) \end{aligned}$$

where $[\cdot]$ denotes the jump across $\Gamma(t)$, \mathbf{I} again the identity tensor and \mathbf{n} the outward normal pointing from $\Omega_{cp}(t)$ into $\Omega_{em}(t)$. The first condition requires continuity of the velocity across the membrane satisfying $\mathbf{u}_1 = \mathbf{u} = \mathbf{u}_2$, and the second condition modeling the jump in the normal component of the stress tensor, accounting for bending and surface tension, which is enriched by the active component associated with actin polymerization associated with the active state of the membrane bound GTPase c_1 . The resulting protrusion force from the last contribution acts in normal direction and its strength is related to c_1 and scaled by the dimensionless quantity Fa . For simplicity we neglect any retraction force. In the current model we also don't consider adhesion explicitly. Possible extensions of the model in these directions are discussed in the Sect. 4.

Typical Helfrich models also contain constraints on cell volume and membrane area. Due to the incompressibility of the fluid in Ω_{cp} the volume constraint is already fulfilled in our approach. Instead of an area or local inextensibility constraint for the membrane we here consider a constant surface tension, which is justified in the content of cell motility as discussed in [Shao et al. \(2010\)](#).

2.2 Diffuse domain approach of the cell motility model

To numerically solve the coupled system for cell shape dynamics, fluid flow and reaction–diffusion along the evolving membrane and within the cytoplasm we construct a diffuse-domain approximation, which is based on the phase-field method. This method introduces an auxiliary field ϕ that distinguishes the cytoplasm from the extracellular matrix. Both are separated from each other by a diffuse layer, which marks the membrane. We define a larger stationary domain $\Omega = \Omega_{cp}(t) \cup \Gamma(t) \cup \Omega_{em}(t)$ in which the phase field variable is defined as

$$\phi(t, \mathbf{x}) := \tanh\left(\frac{r(t, \mathbf{x})}{\sqrt{2}\varepsilon}\right) \tag{12}$$

where ε characterizes the thickness of the diffuse interface and $r(t, \mathbf{x})$ denotes the signed-distance function between $\mathbf{x} \in \Omega$ and its nearest point on $\Gamma(t)$. Depending on r we label the cytoplasm with $\phi \approx 1$ and the extracellular matrix with $\phi \approx -1$. $\Gamma(t)$ is implicitly defined by the zero level set of ϕ .

The dynamics of the cell is now governed by equations that couple this field to the actual physical degrees of freedom along the membrane, in the cytoplasm and the extracellular matrix. All quantities defined within the cytoplasm, within the extracellular matrix and along the membrane are extended to the larger domain Ω and the governing equations are reformulated using the phase field variable. This allows to circumvent the numerical subtleties in solving differential equations on evolving surfaces or within evolving domains. A general mathematical description for the use of the phase-field method to solve such coupled systems was introduced by [Li et al. \(2009\)](#), [Rätz and Voigt \(2006\)](#), and [Teigen et al. \(2009\)](#) which gives the formal verification of the derived model.

Phase-field methods have already been used to model the dynamics of cell membranes, however most studies only consider minimization of the Helfrich energy with constraints on cell volume and membrane area, see e.g. [Du et al. \(2006\)](#). Other fundamental components of cell membranes which include lipids, proteins and cholesterol and their interplay on the morphology, structure and dynamics of membranes are considered by [Allain \(2004\)](#), [Lowengrub et al. \(2009\)](#), [Wang and Du \(2008\)](#). Also the coupling of the dynamics with the surrounding fluid has been modeled ([Biben et al. 2005](#)), as well as effects due to adhesion ([Das and Du 2008](#)). More recently by [Shao et al. \(2012\)](#), and [Shao et al. \(2010\)](#) protrusion and contraction forces are considered to study cell morphodynamics using a phase-field method.

The diffuse nondimensional Helfrich energy reads

$$\begin{aligned} \mathcal{E}(\phi) = & \frac{1}{2\varepsilon} \frac{1}{\text{Be}} \int_{\Omega} \left(\varepsilon \Delta \phi - \frac{1}{\varepsilon} (\phi^2 - 1)(\phi + H_0) \right)^2 dx \\ & + \frac{1}{\text{Ca}} \int_{\Omega} \left(\frac{\varepsilon}{2} |\nabla \phi|^2 + \frac{1}{4\varepsilon} (\phi^2 - 1)^2 \right) dx. \end{aligned} \tag{13}$$

In [Du et al. \(2005a,b\)](#) formal convergence for $\varepsilon \rightarrow 0$ to Eq. (7) could be shown. A thermodynamical consistent phase field approach based on this energy was proposed by [Du et al. \(2007\)](#), [Du et al. \(2009\)](#), and [Ryham et al. \(2012\)](#). Combining this approach with the active protrusion force leads to the nondimensional Navier–Stokes equation

$$\begin{aligned} \partial_t \mathbf{u} + (\mathbf{u} \cdot \nabla) \mathbf{u} &= -\nabla p + \frac{1}{\text{Re}} \Delta \mathbf{u} \\ &+ \frac{1}{\text{ReBe}} g \nabla \phi - \frac{1}{\text{ReCa}} f \nabla \phi + \frac{\lambda_1}{\text{Re}} \nabla \phi - \frac{1}{\text{ReFa}} c_1 \nabla \phi \quad (14) \\ \nabla \cdot \mathbf{u} &= 0 \quad (15) \end{aligned}$$

now defined in Ω . We use the same dimensionless quantities as before: the bending capillary number Be , which was similarly defined by [Biben et al. \(2005\)](#), and [Salac and Miksis \(2011\)](#), the capillary number Ca and the active surface force number Fa , which characterizes the strength of the cell protrusion. All these quantities and their relation to physical parameters will be explained in Sect. 2.3. The evolution of ϕ is given by the system of dimensionless equations

$$\partial_t \phi + \mathbf{u} \cdot \nabla \phi = -\delta \left(\frac{1}{\text{Be}} g - \frac{1}{\text{Ca}} f + \lambda_1 \right) \quad (16)$$

$$g = \Delta f_c - \frac{1}{\varepsilon^2} (3\phi^2 + 2H_0\phi - 1) f_c \quad (17)$$

$$f_c = \varepsilon \Delta \phi - \frac{1}{\varepsilon} (\phi^2 - 1)(\phi + H_0) \quad (18)$$

$$f = \varepsilon \Delta \phi - \frac{1}{\varepsilon} (\phi^2 - 1)\phi \quad (19)$$

$$\lambda_1 = \frac{1}{|\Omega|} \int_{\Omega} \left(\frac{1}{\text{Ca}} f - \frac{1}{\text{Be}} g \right) dx, \quad (20)$$

see [Du et al. \(2005a, 2006\)](#), and [Du and Zhang \(2008\)](#) for a detailed derivation. Equation (16) can be considered as an advection equation for the phase field ϕ , with a regularizing right hand side, with a small numerical parameter δ . Although Eq. (15) theoretically guarantees incompressibility and thus a constant volume, within the phase-field approximation a Lagrange multiplier λ_1 is introduced to enforce the volume constraint explicitly. This approach was proposed by [Du et al. \(2009\)](#) and is certified by our numerical experiments. Formal matched asymptotic analysis results showing the convergence to the sharp interface equations are not available. However numerical convergence studies by [Du et al. \(2005a\)](#), [Du et al. \(2006\)](#), and [Du and Zhang \(2008\)](#) confirm the phase-field approximation without the protrusion force.

We now formulate the minimal reaction–diffusion system within a diffuse domain description. Following [Li et al. \(2009\)](#), Eq. (1) in Ω_{cp} can be reformulated in Ω as follows

$$\partial_t (\psi C) + \nabla \cdot (\psi \mathbf{u} C) = D_C \nabla \cdot (\psi \nabla C) - \gamma |\nabla \psi| q(c_1, c_2, C), \quad (21)$$

with $\psi = \frac{1}{2}(1 + \phi)$ a rescaled phase-field function, which serves as an approximation of the characteristic function of $\Omega_{cp}(t)$, $\psi \approx 1$ in the cytoplasm and $\psi \approx 0$ in the extracellular matrix. In order to extend Eqs. (2) and (3) to Ω , we use the diffuse interface approach proposed by Rätz and Voigt (2006)

$$\partial_t(|\nabla\phi|c_1) + \nabla \cdot (|\nabla\phi|\mathbf{u}c_1) = d_{c_1}\nabla \cdot (|\nabla\phi|\nabla c_1) + \gamma|\nabla\phi|h(c_1, c_2) \quad (22)$$

$$\begin{aligned} \partial_t(|\nabla\phi|c_2) + \nabla \cdot (|\nabla\phi|\mathbf{u}c_2) &= d_{c_2}\nabla \cdot (|\nabla\phi|\nabla c_2) - \gamma|\nabla\phi|h(c_1, c_2) \\ &+ \gamma|\nabla\phi|q(c_1, c_2, C) \end{aligned} \quad (23)$$

Formal convergence to the sharp interface equations can be achieved following the general treatment by Li et al. (2009), Rätz and Voigt (2006), and Teigen et al. (2009).

In this form we have derived a coupled system of Eqs. (14)–(23), all defined in the stationary domain Ω . The primary unknowns are velocity, \mathbf{u} , pressure p , phase-field variable ϕ , and the concentrations c_1 , c_2 and C . The quantities g , f and f_c are introduced to reformulate the higher order equation for ϕ into a system of second order equations, and λ_1 and ψ are the Lagrange parameter, introduced to fulfill the volume constraint, and a rescaled phase-field function, respectively.

2.3 Parameters

The parameters in our model follow either from experimental measurements or other simulation approaches. In order to relate the dimensionless numbers to measured values we introduce a characteristic length $R_0 = 5 \times 10^{-6}$ m, a typical cell radius and a characteristic velocity $v_0 = 0.14 \times 10^{-6}$ m/s, a typical velocity of a moving cell, see e.g. Shao et al. (2012), Shao et al. (2010) and the references therein. We further consider the density of the cytoplasm $\rho = 10^3$ kg/m³, which corresponds to that of water. As already mentioned, for simplicity we consider a constant value for the viscosity in the cytoplasm and the extracellular matrix, which is estimated to be $\mu = 10$ Pa s. For the Reynold number $Re = \rho R_0 v_0 / \mu$ we thus obtain $Re = 7 \times 10^{-11}$, which is much smaller than the considered values by Biben et al. (2005), Ryham et al. (2012), and Salac and Miksis (2011), where $Re = 10^{-3}$ is used. To allow for comparison with these studies we also use $Re = 10^{-3}$ in our simulations. The bending capillary number Be is defined by $Be = 4\sqrt{2}/3 \mu v_0 R_0^2 / b_N$ with bending stiffness b_N and the capillary number Ca is defined by $Ca = 2\sqrt{2}/3 \mu v_0 / \sigma$ with surface tension σ . For $b_N = 10^{-17}$ J and $\sigma = 5 \times 10^{-6}$ N/m, which are measured for Dictyostelium cells by Simson et al. (1998) and used by Shao et al. (2010) we obtain $Be = 6.6$ and $Ca = 0.264$. For simplicity we neglect the spontaneous curvature and set $H_0 = 0$ in all computations. Finally the active surface force number $Fa = \mu v_0 / (\alpha R_0)$ characterizes the cell protrusion. The corresponding parameter is denoted by α , which has the dimension N/m² and measures the strength of the protrusion. As this is an effective term there are no experimental data available for α . We define the strength of the protrusion force to be in the same order as the elasticity force due to bending. With $\alpha = 5.6$ N/m² we obtain $Fa = 0.05$ and together with the other parameters the considered characteristic velocity v_0 . The diffusion coefficients along the membrane are 7×10^{-13} m²/s and within the cytoplasm 1.4×10^{-11} m²/s, see Rätz and Röger

Table 1 Mechanical and chemical parameters

Symbol	Description	Value
R_0	Typical cell radius	5×10^{-6} m
v_0	Typical velocity of crawling cell	0.14×10^{-6} m/s
t_0	Characteristic time	35.714 s
ρ	Fluid density	10^3 kg/m ³
μ	Dynamic viscosity of the fluid	10 Pa s
b_N	Bending rigidity	$10^{-18} - 10^{-17}$ J
σ	Surface tension	$10^{-6} - 10^{-5}$ N/m
α	Coefficient protrusion force	0.39 N/m ² and 5.6 N/m ²
ϵ	Boundary layer parameter	0.03
δ	Regularization parameter	$\frac{\delta}{Be} = 0.01$
D_C	Diffusion coefficient of cytoplasm	20
d_{c_1}	Diffusion coefficient along the membrane for c_1	1
d_{c_2}	Diffusion coefficient along the membrane for c_2	1
a_1	Kinetic coefficient	0
a_2	Kinetic coefficient	160
a_3	Kinetic coefficient	1
a_4	Membrane attachment parameter	0.333
a_5	Membrane detachment parameter	10
b_1	Kinetic parameter	20
b_2	Kinetic parameter	0.5
γ	Scaling parameter	400

The values for b_N correspond to measurements for artificial vesicles, erythrocytes, neutrophils and dictyostelium (Evans and Rawicz 1990; Simson et al. 1998; Strey and Peterson 1995; Zhelev et al. 1994). The values for σ follow from Simson et al. (1998). The boundary layer parameter ϵ is a numerical parameter and determines the width of the diffuse interface. The regularization parameter δ is chosen to depend on Be , see Ryham et al. (2012). All parameters of the reaction–diffusion system are given in dimensionless form. The diffusion coefficients are defined as follows $D_C = \tilde{D}_C/\tilde{d}_{c_1}$ and $d_{c_1} = \tilde{d}_{c_1}/\tilde{d}_{c_1} = 1$, $d_{c_2} = \tilde{d}_{c_2}/\tilde{d}_{c_1} = 1$, where the $\tilde{\cdot}$ notation denotes the dimensionful diffusion coefficients. Together with kinetic parameters a_i , b_i and γ obtained from Rätz and Röger (2013) they lead to a Turing instability

(2012) and the references therein. Realistic reaction parameters are not available, the parameters used follow from a stability analysis of the system leading to a Turing instability, see Rätz and Röger (2013). All parameters used in the simulations are given in Table 1.

2.4 Numerical approach

The systems of partial differential equations are discretized using the adaptive finite element toolbox AMDiS (Vey and Voigt 2007; Voigt and Witkowski 2012). We restrict our simulations to the two-dimensional case and use an adaptively refined triangular mesh with a high resolution along the cell membrane to guarantee at least five grid points across the diffuse interface. We further explore an operator splitting approach

allowing to solve the subproblems of the flow field, the phase-field evolution, the Lagrange multiplier and the reaction–diffusion problem separately in an iterative process. A P^2/P^1 Taylor-Hood element is used for the flow problem, all other quantities are discretized in space using P^2 elements. In time a semi-implicit discretization is used, which together with an appropriate linearization of the involved non-linear terms leads to a set of linear systems in each time step, for which the direct unsymmetric multifrontal method UMFPACK is used.

We split the time interval $I = [0, T]$ into equidistant time instants $0 = t_0 < t_1 < \dots$ and define the time steps $\tau := t_{n+1} - t_n$. We use $\tau = 10^{-3}$ for all computations. Of course, adaptive time steps may also be used. We define the discrete time derivative $d_t^{.n+1} := (.^{n+1} - .^n)/\tau$, where the upper index denotes the time step number.

The numerical approach for each subproblem is adapted from existing algorithms for the Navier–Stokes problem, the Helfrich model and reaction–diffusion models. In each time step we solve:

1. the flow problem for \mathbf{u}^{n+1} and p^{n+1}

$$\begin{aligned}
 d_t \mathbf{u}^{n+1} + (\mathbf{u}^n \cdot \nabla) \mathbf{u}^{n+1} &= -\nabla p^{n+1} + \frac{1}{\text{Re}} \Delta \mathbf{u}^{n+1} \\
 &+ \frac{1}{\text{ReBe}} g^n \nabla \phi^n - \frac{1}{\text{ReCa}} f^n \nabla \phi^n + \frac{1}{\text{Re}} \lambda_1^n \nabla \phi^n \\
 &- \frac{1}{\text{ReFa}} c^n \nabla \phi^n \\
 \nabla \cdot \mathbf{u}^{n+1} &= 0
 \end{aligned}$$

2. the phase field evolution for ϕ^{n+1}

$$\begin{aligned}
 d_t \phi^{n+1} + \mathbf{u}^{n+1} \cdot \nabla \phi^{n+1} &= \delta \left(\frac{1}{\text{Be}} g^{n+1} - \frac{1}{\text{Ca}} f^{n+1} + \lambda_1^n \right) \\
 g^{n+1} &= \Delta f_c^{n+1} - \frac{1}{\varepsilon^2} \left(3(\phi^{n+1})^2 + 2H_0 \phi^{n+1} - 1 \right) f_c^{n+1} \\
 f_c^{n+1} &= \varepsilon \Delta \phi^{n+1} - \frac{1}{\varepsilon} \left((\phi^{n+1})^2 - 1 \right) \left(\phi^{n+1} + H_0 \right) \\
 f^{n+1} &= \varepsilon \Delta \phi^{n+1} - \frac{1}{\varepsilon} \left((\phi^{n+1})^2 - 1 \right) \phi^{n+1}
 \end{aligned}$$

We further linearize the non-linear terms by a Taylor expansion of order one, e.g. $((\phi^{n+1})^2 - 1)\phi^{n+1} = ((\phi^n)^2 - 1)\phi^n + (3(\phi^n)^2 - 1)(\phi^{n+1} - \phi^n)$.

3. the Lagrange multiplier λ_1^{n+1}

$$\lambda_1^{n+1} = \int_{\Omega} \left(\frac{1}{\text{Ca}} f^{n+1} - \frac{1}{\text{Be}} g^{n+1} \right) dx + \frac{1}{2\tau} \left(\mathcal{V}(\phi^{n+1}) - \mathcal{V}_0 \right).$$

This approach uses an additional penalty term, as proposed by [Du et al. \(2006\)](#). \mathcal{V}_0 denotes the desired cell volume and $\mathcal{V}(\phi^{n+1}) = \int_{\Omega} \phi^{n+1} dx$ its actual state. The penalty parameter is related to the time step size τ .

4. the concentrations C^{n+1} , c_1^{n+1} and c_2^{n+1}

$$\begin{aligned}
 d_t (\psi^{n+1} C^{n+1}) + \nabla \cdot (\psi^{n+1} \mathbf{u}^{n+1} C^{n+1}) &= D_C \nabla \cdot (\psi^{n+1} \nabla C^{n+1}) \\
 &\quad - \gamma |\nabla \psi^{n+1}| q (c_1^{n+1}, c_2^{n+1}, C^{n+1}) \\
 d_t (|\nabla \phi^{n+1}| c_1^{n+1}) + \nabla \cdot (|\nabla \phi^{n+1}| \mathbf{u}^{n+1} c_1^{n+1}) &= d_{c_1} \nabla \cdot (|\nabla \phi^{n+1}| \nabla c_1^{n+1}) \\
 &\quad + \gamma |\nabla \phi^{n+1}| h (c_1^{n+1}, c_2^{n+1}) \\
 d_t (|\nabla \phi^{n+1}| c_2^{n+1}) + \nabla \cdot (|\nabla \phi^{n+1}| \mathbf{u}^{n+1} c_2^{n+1}) &= d_{c_2} \nabla \cdot (|\nabla \phi^{n+1}| \nabla c_2^{n+1}) \\
 &\quad - \gamma |\nabla \phi^{n+1}| h (c_1^{n+1}, c_2^{n+1}) \\
 &\quad + \gamma |\nabla \phi^{n+1}| q (c_1^{n+1}, c_2^{n+1}, C^{n+1})
 \end{aligned}$$

with $\psi^{n+1} = \frac{1}{2}(1 + \phi^{n+1})$. We again further linearize the non-linear terms q and h according to the proposed approach in [Rätz and Röger \(2012\)](#).

We start with appropriate initial conditions for \mathbf{u} , c_1 , c_2 , C and ϕ and set homogeneous Neumann boundary conditions for c_1 , c_2 , C , g , f_c and f , and Dirichlet boundary conditions $\mathbf{u} = 0$ and $\phi = -1$ on $\partial\Omega$. The numerical approach for each subproblem has already been validated elsewhere. We therefore consider here only convergence tests for the coupled problem. After reaching the desired pattern on the cellular membrane to distinguish between cell front and rear, which can be obtained by solving subproblem 4 on a stationary circular shape using the proposed parameters by [Rätz and Röger \(2013\)](#), the whole system is solved. A deformation of the cell can be observed and a movement in the direction of the cell front. After an initialization state a stationary form and a constant velocity is reached. We measure the following quantities: the x_1 -coordinate of the center of mass, which is defined as $x_c = \int_{\Omega_{cp}} x_1 \, dx / \int_{\Omega_{cp}} 1 \, dx$, where $\mathbf{x} = (x_1, x_2)$, the circularity of the cell, which is defined as the quotient of the perimeter of an area-equivalent circle and the perimeter of the cell $circ = 2(\int_{\Omega_{cp}} \pi \, dx)^{1/2} / P_b$, with the perimeter P_b obtained by integration over a contour filter in ParaView, the velocity of the cell, which is defined as $u_{cell} = |\mathbf{u}(x_c, x_2)|$, and the bending energy $\mathcal{E}_{bending} = \frac{1}{2\epsilon} \frac{1}{Be} \int_{\Omega} (\epsilon \Delta \phi - \frac{1}{\epsilon} (\phi^2 - 1)(\phi + H_0))^2 \, dx$. All defined quantities are time dependent. A relative error can be defined to measure their temporal evolution. We use the following error norm: $\|e\|_2 = ((\sum_I |q_{t,ref} - q_t|^2) / (\sum_I |q_{t,ref}|^2))^{1/2}$, where q_t is the temporal evolution of quantity q . The solution on the finest grid serves as reference solution $q_{t,ref}$. Table 2 shows the relative error norms as well as the relative order of convergence (ROC) for the desired quantities if ϵ is reduced. Together with ϵ we also refine the mesh size to guarantee the same number of grid points within the diffuse interface layer for all simulations and the time step to ensure the same relation between mesh size and time step. The time interval is $I = [0, 3.5]$, which corresponds to an end time of $T = 123s$. Other parameters are obtained from Table 1, in particular $b_N = 10^{-17} J$, $\sigma = 5 \times 10^{-6} \text{ N/m}$ and $\alpha = 5.6 \text{ N/m}^2$ which corresponds to $Be = 6.6$, $Ca = 0.264$ and $Fa = 0.05$, respectively. We see at least first order

Table 2 Relative error norms and convergence orders for critical parameters

ϵ	Center of mass x_c		Cell velocity u_{cell}		Circularity $circ$		Energy $\mathcal{E}_{bending}$	
	$\ e\ _2$	ROC	$\ e\ _2$	ROC	$\ e\ _2$	ROC	$\ e\ _2$	ROC
0.060	0.0530		0.1895		0.0094		0.1177	
0.042	0.0168	3.3081	0.0630	3.1734	0.0075	0.6807	0.0771	1.2190
0.030	0.0044	3.8812	0.0272	2.4244	0.0045	1.4408	0.0334	2.4180
0.021	0.0004	6.7472	0.0094	2.9673	0.0024	1.7358	0.0127	2.7072

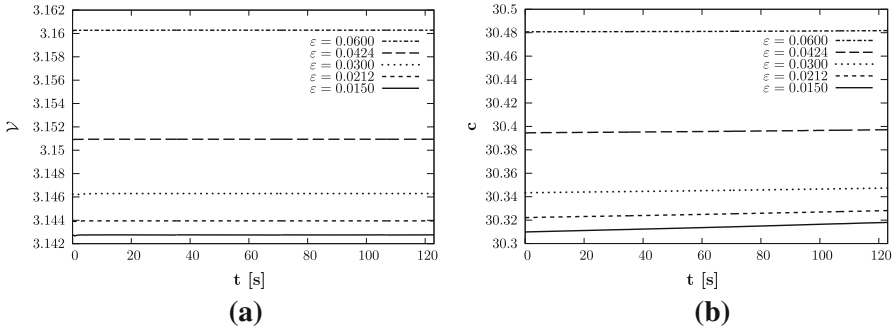


Fig. 3 Evolution of cell volume and mass of the GTPases for various parameters ϵ . **a** Volume conservation. **b** Mass conservation

convergence, the higher numbers in ROC for x_c , u_{cell} and $\mathcal{E}_{bending}$ are probably due to fortunate circumstances.

As a further consistency test, we consider conservation of mass and cell volume. The total mass is measured as $c = \int_{\Omega} (c_1 + c_2)|\nabla\psi| dx + \int_{\Omega} C\psi dx$ and the volume is estimated as $\mathcal{V} = \int_{\Omega} \psi dx$. Figure 3 shows the evolution of both quantities over time for the same parameters as above, and demonstrate the required conservation.

3 Results

We consider the dependency of cell motility on various parameters: the bending stiffness b_N , the surface tension σ and the protrusion force parameter α . Modifying the reaction–diffusion parameters also allows to form either lamellipodia- or filopodia-like structures, which we demonstrate in an example. We further extend the model to consider chemotaxis and compute the cell path according to a varying chemotaxis signal.

3.1 Mechanical dependency of motile cells

As initial condition we consider a circular membrane of radius 1. To speed up the development of the Turing pattern the simulation starts with a constant value $C = 9.25$ in $\Omega_{cp}(0)$, $c_1 = 0.1758$ and $c_2 = 0.2186$ on the right hand side of the cellular

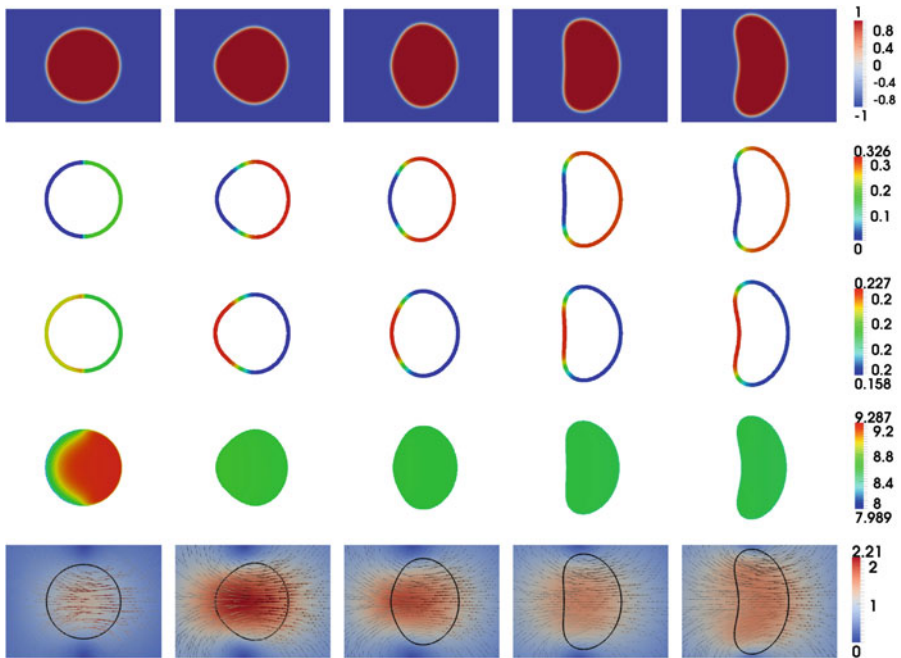


Fig. 4 Cell movement. *First row* shape of the cell at different times evolving from *left to right*. Shown is the phase field variable ϕ , *second row* concentration of c_1 on cell membrane, *third row* concentration of c_2 on cell membrane, *fourth row* concentration of C in the cytoplasm, *fifth row* magnitude and direction of \mathbf{u} . The maximum of $|\mathbf{u}|$ corresponds to 0.31×10^{-6} m/s, which is in good agreement with the value reported by [Shao et al. \(2012\)](#). To visualize the concentrations along the cell membrane or in the cytoplasm the values of c_1 and c_2 and C are shown at the $[-0.9, 0.9]$ and $[0, 1]$ level sets of the phase field variable, respectively. The times t shown are 0.013, 0.3, 0.6, 1.2 and 8 which correspond to 4.64, 10.71, 21.43, 42.86 and 250 s, from *left to right*

membrane and $c_1 = 0$ and $c_2 = 0$ on the left hand side. After a few iteration of the whole system a stable Turing pattern with the desired polarity is formed. The resulting protrusion force leads to a movement to the right and a deformation of the cell shape forming a lamellipodia-like structure. Figure 4 shows the time evolution of the phase field variable ϕ and the concentrations c_1 , c_2 and C , respectively. The maxima of c_1 which signals the polymerization of the actin filament meshwork in our model, is sharply localized at the cell front. The concentration profile of c_2 is less pronounced and the concentration of C within the cytoplasm shows only a small gradient towards the cell front. Both c_2 and C do not directly correspond to the cell movement in the considered model. We also show the velocity, which reaches after the acceleration of the cell at the beginning a maximum before it is slowed down into a stationary profile leading to a stationary cell shape moving with constant velocity. In this state the shear stress and the stress corresponding to the Helfrich forces are in balance. The simulation is performed with $b_N = 10^{-17} J$, $\sigma = 5 \times 10^{-6}$ N/m and $\alpha = 5.6$ N/m².

The stationary shape strongly depends on these parameters. To quantify the dependency Fig. 5 shows the obtained stationary cell shapes for different bending stiffness b_N and different surface tension σ . For Fig. 5a we vary the bending stiffness parameter

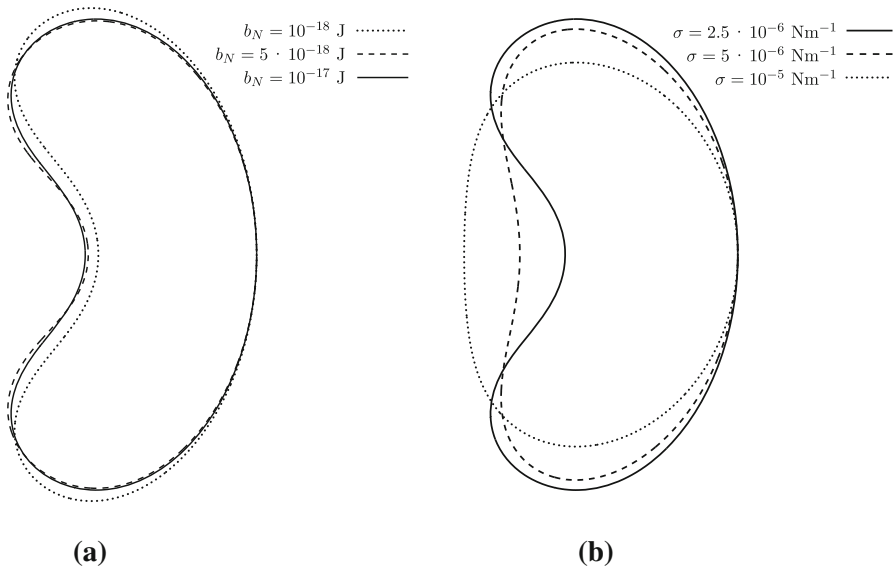


Fig. 5 Contour of the stationary cell shapes for bending and stiffness values proposed in Table 1. **a** $\sigma = 2.5 \times 10^{-6}$ N/m. **b** $b_N = 10^{-17}$ J

and use a constant surface tension $\sigma = 2.5 \times 10^{-6}$ N/m. For Fig. 5b, we use different values for the surface tension and keep the bending stiffness $b_N = 10^{-17}$ J constant. $\alpha = 5.6$ N/m² is kept constant in all simulations. As expected the cell remains more circular as stronger the bending stiffness and surface tension. More important, the results indicate that the influence of bending stiffness compared to surface tension is relatively small.

We now consider the influence of the protrusion force on the stationary cell shape. Figure 6c shows the stationary cell shapes for different protrusion coefficients α . The other parameters are $b_N = 10^{-17}$ J and $\sigma = 5 \times 10^{-6}$ N/m.

3.2 Formation of filopodia-like structures

In the previous example the diffusion coefficients and kinetic parameters are chosen to form a Turing pattern which defines a polarity to distinguish between cell front and cell rear. Different parameters can lead to different patterns. We here demonstrate this by using again a circular initial shape of radius 1, a constant value of $C = 9.25$ in the cytoplasm and random initial conditions for c_1 and c_2 within $[0.1758 - 0.01, 0.1758 + 0.01]$ and $[0.2186 - 0.01, 0.2186 + 0.01]$, respectively. We here also modify the diffusion coefficient d_{c_2} along the membrane, which is set to be $d_{c_2} = 750$ and now differs from d_{c_1} . The second change in parameters concerns the active surface force number Fa , which now becomes $Fa = 0.71$, corresponding to $\alpha = 0.39$ N/m². The elastic parameters of the membrane are set to be $b_N = 10^{-18}$ J and $\sigma = 10^{-6}$ N/m. Figure 7 shows the time evolution of the phase field variable, the concentrations of c_1 and c_2 along the membrane, the concentration of C within the cytoplasm as well as the velocity field. Due to the developing of various maxima in c_1 the cell only deforms

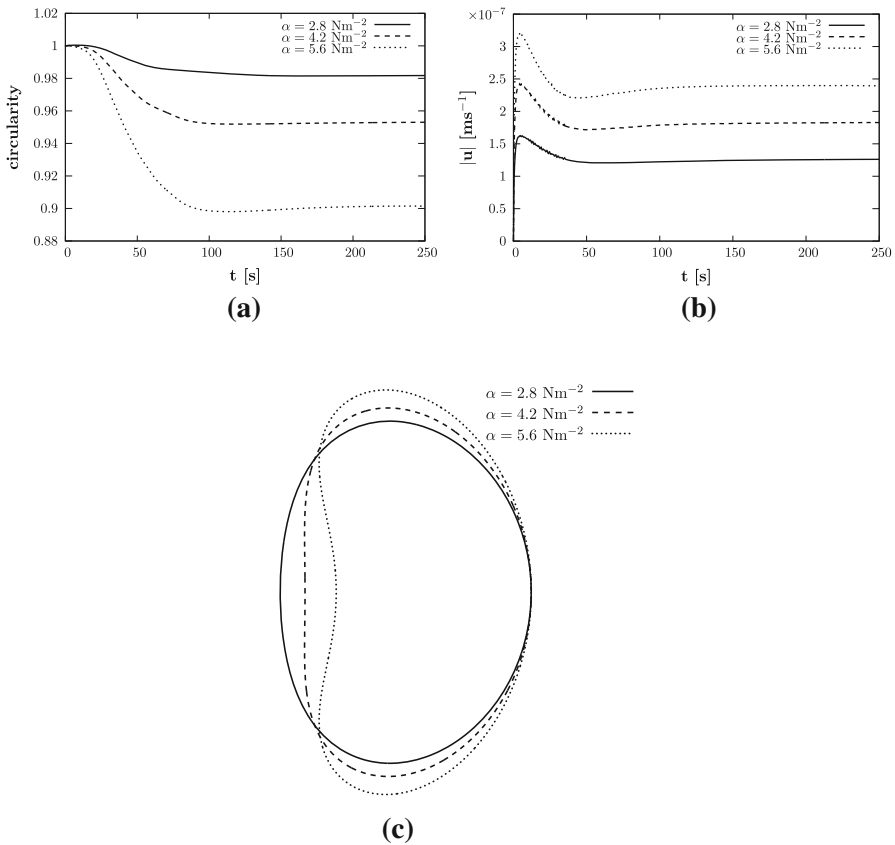


Fig. 6 Variation of α leads to different cell shapes, as larger the protrusion force as stronger is the deformation and as faster the cell movement. **a** Circularity, **b** velocity of the center of mass and **c** the reached stationary shape

but does not move into one direction. In contrast to our previous simulations we also achieve a pattern in C . A stationary shape is not reached within the simulation time.

3.3 Reaction to spatial signals

It remains to be determined to what extent such an intrinsic polarization mechanism contributes under physiological conditions where cell polarization is controlled by spatial signals. In neutrophils, the actin cytoskeleton plays an important role in the amplification of the spatial signal provided by gradients of chemoattractants. Thus, the cytoskeleton-dependent positive feedback loop could also be used as a powerful signal amplification mechanism that amplifies a small initial asymmetry in the distribution of polarity inducers, thereby establishing the polarity axis toward a physiologically relevant orientation.

To demonstrate this effect we modify Eq. (2) by adding $\nabla_{\Gamma} \cdot (c_1 \nabla_{\Gamma} \tilde{c})$, with \tilde{c} a given concentration of a chemoattractant in the extracellular matrix. A similar approach has

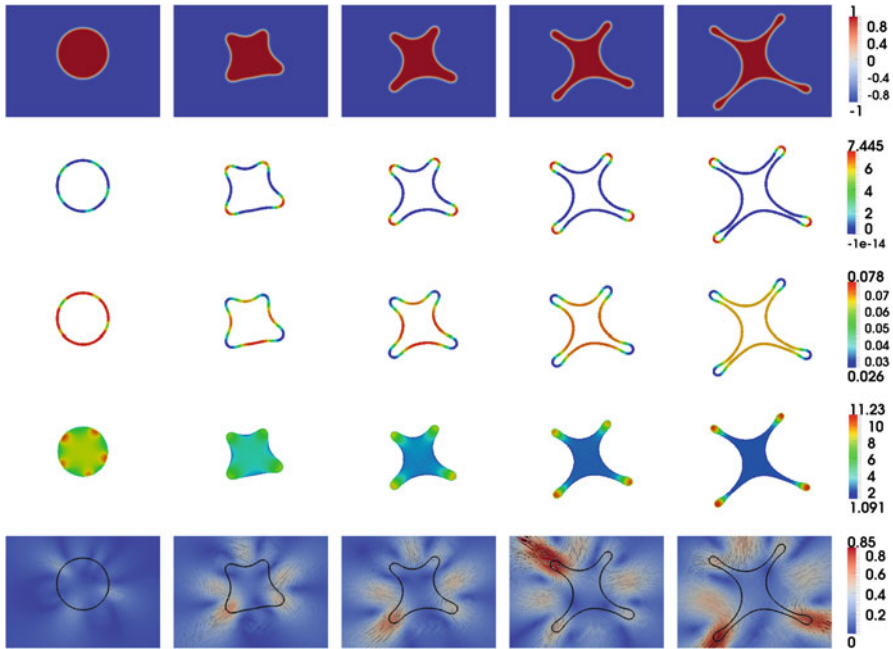


Fig. 7 First row shape of the cell at different times evolving from left to right. Shown is the phase field variable ϕ , second row concentration of c_1 on cell membrane, third row concentration of c_2 on the cell membrane, fourth row concentration of C within the cytoplasm and last row velocity field. The concentrations along the cell membrane and in the cytoplasm are shown at the $[-0.9, 0.9]$ and $[0, 1]$ level sets of the phase field variable, respectively. The times t corresponding to the columns are 0.1, 1, 2, 3 and 4 and are equal at 3.6, 35.7, 71.4, 107.1 and 142.9 s, from left to right

been used by Elliott et al. (2012), and Landsberg et al. (2011). The modified diffuse interface equation reads

$$\begin{aligned} \partial_t (|\nabla\phi|c_1) + \nabla \cdot (|\nabla\phi|\mathbf{u}c_1) &= d_{c_1} \nabla \cdot (|\nabla\phi|\nabla c_1) + \gamma |\nabla\phi| h(c_1, c_2) \\ &+ \nabla \cdot (|\nabla\phi|c_1 \mathcal{P}_\phi \nabla \tilde{c}) \end{aligned} \tag{24}$$

where $\mathcal{P}_\phi = \mathbf{I} - \frac{\nabla\phi \cdot \nabla\phi}{|\nabla\phi|^2}$ denotes the projection operator towards the interface, with the identity matrix \mathbf{I} .

To illustrate the applicability of the approach we use different modes of \tilde{c} and its gradient:

1. $\nabla\tilde{c} = \xi(\cos \omega t, \sin \omega t)^T$, the chemoattractant rotates with the angular velocity ω ,
2. $\nabla\tilde{c} = \xi(1, \sin \omega t)^T$, the chemoattractant changes its direction in a sinusoidal way,
3. $\nabla\tilde{c} = \xi \mathcal{R}(\chi^{\lfloor \frac{n}{\vartheta} \rfloor + 1}) \cdot \nabla\tilde{c}(\chi^{\lfloor \frac{n}{\vartheta} \rfloor})$, the chemoattractant randomly changes its direction by a specific angle ω . The random variable χ is determined every ϑ -th time step and has the possible values $\{-\omega, 0, \omega\}$. \mathcal{R} denotes a rotation matrix and $\nabla\tilde{c}(\chi^{\lfloor \frac{n}{\vartheta} \rfloor})$ determines the old direction of the chemoattractant. Similar rules are proposed by Elliott et al. (2012).

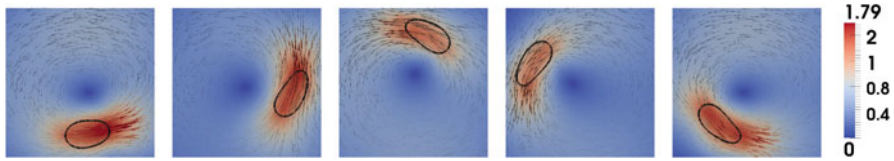


Fig. 8 Cell responds to a rotating spatial signal leading to a rotation, corresponding to case 1. The cell shape and velocity in the cytoplasm and in the extracellular matrix is shown for times t equal 21.4, 107.1, 214.3, 321.4 and 428.6 s, from *left to right*

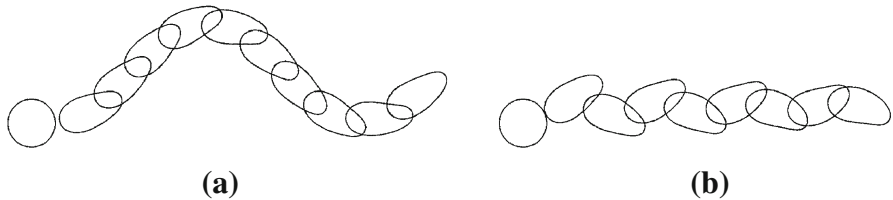


Fig. 9 Cell responds to a sinusoidal spatial signal, corresponding to case 2. **a** $\omega = 0.014/s$. **b** $\omega = 0.056/s$

The parameter ξ models the strength of the chemotactic signal, which is set to $\xi = 5$ in all simulations and thus dominates the reaction–diffusion system, leading to a pronounced maxima of c_1 in the direction of the strongest gradient of the chemoattractant. Fig. 8, corresponding to case 1, shows the resulting rotation of the cell together with the velocity field. The maxima in c_1 always points in the direction of the highest gradient of the chemoattractant. We again observe the formation of a stationary shape here influenced by the spatial signal. Figure 9, corresponding to case 2, shows the evolution of the cell from $t = 0s$ to $t = 428 s$ for $\omega = 0.014/s$ (Fig. 9a) and $\omega = 0.056/s$ (Fig. 9b). The last configuration, corresponding to case 3, is shown in Fig. 10 demonstrating a more chaotic movement, which becomes stronger for larger ω and smaller ϑ .

4 Discussion

The movement of crawling cells is described using an effective model for the reorganization of the actin cytoskeleton, which is combined with a Helfrich model for the cell membrane and streaming within the cytoplasm and the extracellular matrix. The actin polymerization leading to cell protrusion is thereby initiated by a membrane-bound active state of the GTPase, as one component of a biochemical network model, taking into account the different dimensionality of the cytoplasm and the cell membrane. The model allows to form Turing pattern in a parameter regime in which diffusion along the membrane can be equal for all components. The used network model is a minimal model with these characteristics and only takes into account the active and inactive state of the membrane-bound GTPase, as well as complexes of cytoplasmic GTPase. However, the minimal model for the GTPases cycle already shows a large variety of different dynamical behavior, which range from sheet-like formation of lamellipodia and the evolution of stationary cell shapes, to fingering phenomena which are

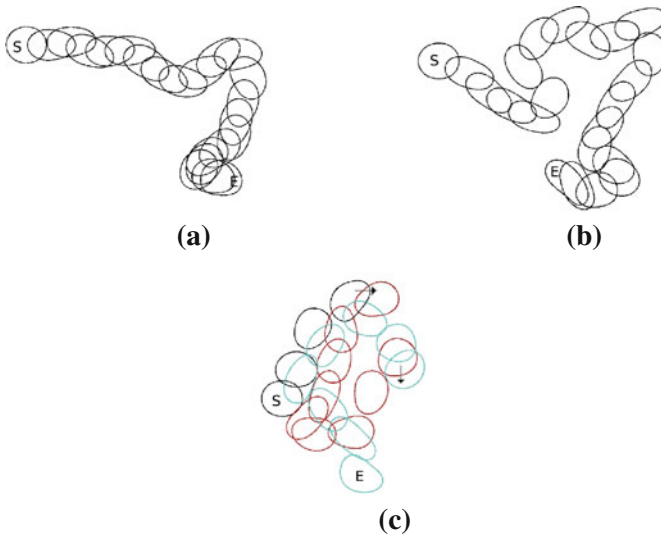


Fig. 10 Cell evolution corresponding to case 3. The starting point is labeled by S and the end point by E . **a** $\omega = 30^\circ$, $\vartheta = 400$. **b** $\omega = 60^\circ$, $\vartheta = 400$. **c** $\omega = 60^\circ$, $\vartheta = 100$

filopodia-like. The difference is achieved by changing the strength of the reaction and the diffusion parameters along the membrane.

The system of equations is formulated in a phase-field approach, which allows for an efficient numerical treatment. Especially the reaction–diffusion model along the membrane and within the cytoplasm can be formulated as a coupled system in a fixed domain using the diffuse interface and diffuse domain approach. The same approach can be applied for more detailed biochemical network models, as e.g. proposed by [Goryachev and Pokhilko \(2008\)](#). Also the protrusion force can be generalized by taking into account various concentrations along the membrane and within the cytoplasm. In addition also a retracting force can be considered. If we denote concentrations along the membrane by c_i and within the cytoplasm by C_i , the general form for the nondimensional Navier–Stokes equation reads

$$\begin{aligned}
 \partial_t \mathbf{u} + (\mathbf{u} \cdot \nabla) \mathbf{u} &= -\nabla p + \frac{1}{\text{Re}} \Delta \mathbf{u} \\
 &+ \frac{1}{\text{ReBe}} g \nabla \phi - \frac{1}{\text{ReCa}} f \nabla \phi + \frac{\lambda_1}{\text{Re}} \nabla \phi \\
 &- \sum_i \frac{1}{\text{ReFa}_i} c_i \nabla \phi - \sum_i \frac{1}{\text{Re}\overline{\text{Fa}}_i} C_i \nabla \phi \quad (25) \\
 \nabla \cdot \mathbf{u} &= 0 \quad (26)
 \end{aligned}$$

with $Fa_i = \mu v_0 / (\alpha_i R_0)$ the active surface force numbers and $\overline{Fa}_i = \mu v_0 / (\overline{\alpha}_i R_0)$ the active bulk force numbers. In [Shao et al. \(2012, 2010\)](#) only the last terms are considered, one for a protrusion and one for a retraction force. The importance of retraction for cell motility is e.g. considered by [Enculescu et al. \(2008\)](#), [Enculescu](#)

et al. (2010) and needs to be taken into account for quantitative comparisons with specific cells.

An additional contribution neglected in the current model is adhesion. The strong influence of adhesion is e.g. considered by Barnhart et al. (2011). In Das and Du (2008) adhesion is modeled in the context of a Helfrich model using an effective contact potential W , as already proposed by Seifert and Lipowsky (1990). W is thereby modeled as a function of distance between the membrane and the substrate, e.g. in Lennard–Jones form $W(\bar{r}) = -((\beta/\bar{r})^\eta - (\beta/\bar{r})^{\eta/2})$, with \bar{r} the signed distance function to the substrate, β and η the thickness of the repulsive region and the rate of change of the adhesion potential, respectively. The generalized diffuse nondimensional Helfrich energy reads

$$\begin{aligned} \mathcal{E}(\phi) = & \frac{1}{2\varepsilon} \frac{1}{\text{Be}} \int_{\Omega} \left(\varepsilon \Delta \phi - \frac{1}{\varepsilon} (\phi^2 - 1)(\phi + H_0) \right)^2 dx \\ & + \frac{1}{\text{Ca}} \int_{\Omega} \left(\frac{\varepsilon}{2} |\nabla \phi|^2 + \frac{1}{4\varepsilon} (\phi^2 - 1)^2 \right) dx \\ & + \frac{1}{Ad} \int_{\Omega} W(\bar{r}) \left(\frac{\varepsilon}{2} |\nabla \phi|^2 + \frac{1}{4\varepsilon} (\phi^2 - 1)^2 \right) dx. \end{aligned} \quad (27)$$

with the adhesion strength number $Ad = 2\sqrt{2}/3 \mu v_0/\omega$, with ω the strength of the adhesion interaction.

To summarize, the introduced model combines the main contributions to cell motility enabling to reproduce its primary phenomenology. The phase-field approach provides an easy to handle and efficient numerical approach to deal with the highly coupled system of equations. The approach can further be extended to incorporate additional phenomena. The simulation results are obtained not for a specific cell type, but within a realistic parameter range spanning a large class of cells and their environment. We therefore expect the model and the numerical approach to be useful also for quantitative simulations of specific cells.

Acknowledgments The work has been funded through grant DFG Vo899/6 and FP7 IRSES 247504. We further acknowledge the provided computing resources at ZIH at TU Dresden.

References

- Allain J, Ben Amar M (2004) Biphasic vesicle: instability induced by adsorption of proteins. *Phys A* 337:531–545
- Altschuler SJ, Angenent SB, Wang Y, Wu LF (2008) On the spontaneous emergence of cell polarity. *Nature* 454:886–889
- Barnhart E, Lee KC, Keren K, Mogilner A, Theriot J (2011) An adhesion-dependent switch between mechanisms that determine mitotic cell shape. *PLOS Biol* 9:e1001059
- Biben T, Kassner K, Misbah C (2005) Phase-field approach to three-dimensional vesicle dynamics. *Phys Rev E* 72:1–15
- Bonito A, Nochetto R, Pauletti M (2011) Dynamics of biomembranes: effect of the bulk fluid. *Math Model Nat Phenom* 6:25–43

- Das S, Du Q (2008) Adhesion of vesicles to curved substrates. *Phys Rev E* 77
- Du Q, Li M, Liu C (2007) Analysis of a phase field Navier–Stokes vesicle–fluid interaction model. *Discrete Contin Dyn Syst Ser B* 8:539–556
- Du Q, Liu C, Ryham R, Wang X (2005) A phase field formulation of the Willmore problem. *Nonlinearity* 18:1249
- Du Q, Liu C, Ryham R, Wang X (2005) Modeling the spontaneous curvature effects in static cell membrane deformations by a phase field formulation. *Commun Pure Appl Anal* 4:537–548
- Du Q, Liu C, Ryham R, Wang X (2009) Energetic variational approaches in modeling vesicle and fluid interactions. *Phys D* 238:923–930
- Du Q, Liu C, Wang X (2006) Simulating the deformation of vesicle membranes under elastic bending energy in three dimensions. *J Comput Phys* 212:757–777
- Du Q, Zhang J (2008) Adaptive finite element method for a phase field bending elasticity model of vesicle membrane deformations. *SIAM J Sci Comput* 30:1634–1657
- Elliott C, Stinner B (2010) A surface phase field model for two-phase biological membranes. *SIAM J Appl Math* 70:2904–2928
- Elliott CM, Stinner B, Venkataraman C (2012) Modelling cell motility and chemotaxis with evolving surface finite elements. *J R Soc Interface* 9:3027–3044
- Enculescu M, Gholami A, Falcke M (2008) Dynamic regimes and bifurcations in a model of actin-based motility. *Phys Rev E* 78:031,915
- Enculescu M, Sabouri-Ghorni M, Danuser G, Falcke M (2010) Modeling of protrusion phenotypes driven by the actin–membrane interaction. *Biophys J* 98:1571–1581
- Evans E, Rawicz W (1990) Entropy-driven tension and bending elasticity in condensed-fluid membranes. *Phys Rev Lett* 64:2094–2097
- Goryachev AB, Pokhilko AV (2008) Dynamics of Cdc42 network embodies a Turing-type mechanism of yeast cell polarity. *FEBS Lett* 582:1437–1443
- Haußer F, Li S, Lowengrub J, Marth W, Rätz A, Voigt A (2013) Thermodynamically consistent models for two-component vesicles (submitted)
- Helfrich W (1973) Elastic properties of lipid bilayers: theory and possible experiments. *Z Naturforsch* 28:693–703
- Jilkine A, Edelstein-Keshet L (2011) A comparison of mathematical models for polarization of single eukaryotic cells in response to guided cues. *PLoS Comput Biol* 7:e1001121
- Landsberg C, Stenger F, Deutsch A, Gelinsky M, Roesen-Wolff A, Voigt A (2011) Chemotaxis of mesenchymal stem cells within 3D biomimetic scaffolds—a modeling approach. *J Biomech* 44:359–364
- Levine H, Rappel WJ (2005) Membrane-bound Turing patterns. *Phys Rev E* 72:061,912
- Li X, Lowengrub J, Raetz A, Voigt A (2009) Solving PDE’s in complex geometries: a diffuse domain approach. *Commun Math Sci* 7:81–107
- Lowengrub J, Xu J, Voigt A (2007) Surface phase separation and flow in a simple model of multicomponent drops and vesicles. *Fluid Dyn Math Proc* 3:13–28
- Lowengrub JS, Rätz A, Voigt A (2009) Phase-field modeling of the dynamics of multicomponent vesicles: spinodal decomposition, coarsening, budding, and fission. *Phys Rev E* 79:031,926
- Maree AFM, Jilkine A, Dawes A, Grieneisen VA, Edelstein-Keshet L (2006) Polarization and movement of keratocytes: a multiscale modelling approach. *Bull Math Biol* 68:1169–1211
- McMahon H, Gallop J (2005) Membrane curvature and mechanisms of dynamic cell membrane remodeling. *Nature* 438:590–596
- Rätz A, Röger M (2012) Turing instabilities in a mathematical model for signaling networks. *J Math Biol* 65:1215–1244
- Rätz A, Röger M (2013) Symmetry breaking in a bulk-surface reaction-diffusion model for signaling networks (preprint)
- Rätz A, Voigt A (2006) PDE’s on surfaces—a diffuse interface approach. *Commun Math Sci* 4:575–590
- Ryham R, Cohen FS, Eisenberg R (2012) A dynamic model of open vesicles in fluids. *Commun Math Sci* 10:1273–1285
- Salac D, Miksis M (2011) A level set projection model of lipid vesicles in general flows. *J Comput Phys* 230:8192–8215
- Seifert U (1997) Configurations of fluid membranes and vesicles. *Adv Phys* 46:13–137
- Seifert U, Lipowsky R (1990) Adhesion of vesicles. *Phys Rev A* 42:4768–4771

- Shao D, Levine H, Rappel WJ (2012) Coupling actin flow, adhesion, and morphology in a computational cell motility model. *PNAS* 109:6851–6856
- Shao D, Rappel WJ, Levine H (2010) Computational model for cell morphodynamics. *Phys Rev Lett* 105:108,104
- Simson R, Wallraff E, Faix J, Niewohner J, Gerisch G, Sackmann E (1998) Membrane bending modulus and adhesion energy of wild-type and mutant cells of *Dictyostelium* lacking talin or cortexillins. *Biophys J* 74:514–522
- Sohn JS, Tseng YH, Li S, Voigt A, Lowengrub JS (2010) Dynamics of multicomponent vesicles in a viscous fluid. *J Comput Phys* 229:119–144
- Strey H, Peterson M (1995) Measurement of erythrocyte-membrane elasticity by flicker eigenmode decomposition. *Biophys J* 69:478–488
- Teigen KE, Li X, Lowengrub J, Wang F, Voigt A (2009) A diffuse-interface approach for modeling transport, diffusion and adsorption/desorption of material quantities on a deformable interface. *Comm Math Sci* 7:1009–1037
- Teigen KE, Song P, Lowengrub J, Voigt A (2011) A diffuse-interface method for two-phase flows with soluble surfactants. *J Comput Phys* 230(2):375–393
- Vanderlei B, Feng JJ, Edelstein-Keshet L (2011) A computational model of cell polarization and motility coupling mechanics and biochemistry. *Multiscale Model Simul* 9:1420–1443
- Veksler A, Gov NS (2007) Phase transitions of the coupled membrane-cytoskeleton modify cellular shape. *Biophys J* 93:3798–3810
- Vey S, Voigt A (2007) Amdis: adaptive multidimensional simulations. *Comput Visual Sci* 10:57–67
- Voigt A, Witkowski T (2012) A multi-mesh finite element method for lagrange elements of arbitrary degree. *J Comput Sci* 3:420–428
- Wang X, Du Q (2008) Modelling and simulations of multi-component lipid membranes and open membranes via diffuse interface approaches. *J Math Biol* 56:347–371
- Wedlich-Soldner R, Altschuler S, Wu L, Li R (2003) Spontaneous cell polarization through actomyosin-based delivery of the Cdc42 GTPase. *Science* 299:1231–1235
- Wedlich-Soldner R, Wai S, Schmidt T, Li R (2004) Robust cell polarity is a dynamic state established by coupling transport and GTPase SIGNALING. *J Cell Biol* 166:889–900
- Zhelev DV, Needham D, Hochmuth R (1994) A novel micropipet method for measuring the bending modulus for vesicle membranes. *Biophys J* 67:720–727
- Ziebert F, Swaminathan S, Aranson IS (2012) Model for self-polarization and motility of keratocyte fragments. *J Roy Soc Interface* 9:1084–1092